JOURNAL OF COMPUTATIONAL PHYSICS **132,** 191–200 (1997)
ARTICLE NO. CP965571

A Chebyshev Collocation Method for Solving Two-Phase Flow Stability Problems

P. A. M. Boomkamp,*,† B. J. Boersma,‡ R. H. M. Miesen,* and G. V. Beijnon*

*Shell Research and Technology Centre, Amsterdam, P.O. Box 38000, 1030 BN Amsterdam, The Netherlands; †University of Twente, P.O. Box 217, 7500 AE Enschede, The Netherlands; ‡Delft University of Technology, Laboratory for Aero- and Hydrodynamics, Rotterdamseweg 145, 2628 AL Delft, The Netherlands

Received January 22, 1996; revised July 11, 1996

This paper describes a Chebyshev collocation method for solving the eigenvalue problem that governs the stability of parallel two-phase flow. The method is based on the expansion of the eigenfunctions in terms of Chebyshev polynomials, point collocation, and the subsequent solution of the resulting generalized eigenvalue problem with the QZ-algorithm. We concentrate on the question how to handle difficulties that arise when these ''standard'' techniques are applied to the stability problem of a thin film of liquid that is sheared by a gas. After discussing this specific problem in detail, it is argued that the method of solution can readily be applied to other two-phase flow configurations as well.

1. INTRODUCTION

One of the oldest topics in fluid dynamics is the study of the generation of water waves by wind, both in the context of deep water and thin films. To predict whether or not waves will form on the air–water interface, fluid dynamicists often make use of the linear theory of hydrodynamic stability [1]. This theory investigates the evolution of an infinitesimally small disturbance of the basic flow, assuming that the growth of such small disturbances gives rise to (finite-amplitude) waves that can be observed experimentally. From a mathematical point of view, the equations governing stability constitute an eigenvalue problem for the wave velocity of the disturbance in question. Since the full eigenvalue problem is difficult to solve, Benjamin [2] presented in the late 1950s a ''quasi-static'' approximation to tackle the air–water stability problem. In this ''divided attack,'' as Benjamin calls it, the stability problem is solved in two successive steps. First the stresses that a gas flow exerts on a solid wavy boundary are calculated; these stresses are then used in the boundary conditions for the equations of motion for the water layer, the solution of which gives the conditions at which small disturbances grow with time.

Today, modern computational facilities allow us to solve the gas–liquid stability problem entirely numerically, thus avoiding the use of asymptotic techniques like Benjamin's divided attack. In a recent paper, Miesen and Boersma [3] show that such a numerical solution offers the possibility to compare the results of a coupled description of the problem, in which the equations of motion for the gas and the liquid are solved simultaneously, with those of the divided attack. In the present paper, we consider the gas–liquid stability problem from a computational rather than a physical point of view; i.e., we discuss the technique for solving the gas–liquid stability problem. Emphasis is on the difficulties that are encountered when a Chebyshev collocation technique is applied to the specific problem of a thin film of liquid that is sheared by a gas. After discussing these difficulties in detail and presenting some illustrating results, it is argued that the same numerical procedure can readily be applied to other two-phase flow configurations as well.

2. FORMULATION

As shown in Fig. 1, we consider a liquid film ($j = 1$) that is at the lower side bounded by a wall, and at the upper side by a gas ($j = 2$). The gas exerts a shear stress τ on the liquid, which sets the liquid into motion. Density and dynamic viscosity are denoted by ρ_j and μ_j, respectively. The coordinates along and perpendicular to the undisturbed interface are x and y, respectively, with the origin of y chosen at the interface.

The stability of the flow configuration in Fig. 1 is investigated by disturbing the primary flow $U_j(y)$, which will be specified further on, infinitesimally [1]. Using the presumptions that the flow is two-dimensional and incompressible, we represent the disturbance velocities (u_j, v_j) in the fluids by the streamfunctions $\Phi_j(x, y, t)$, so that $(u_j, v_j) = (\partial\Phi_j/\partial y, -\partial\Phi_j/\partial x)$ [4]. Because the primary flow $U_j(y)$ only depends on the y-coordinate, we assume these streamfunctions have the form

$$\Phi_j(x, y, t) = \phi_j(y)e^{i\alpha(x-ct)}, \tag{1}$$

where i is the imaginary unit, α is a real wavenumber, and

0021-9991/97 $25.00

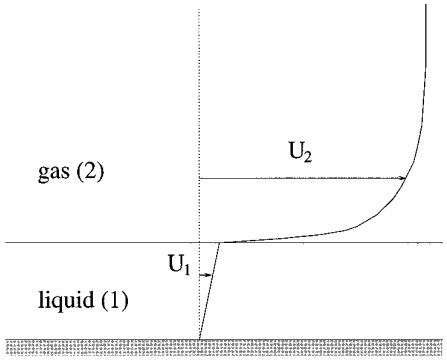

FIG. 1. A thin film of liquid sheared by a gas.

c is the complex wave velocity. The real part of c gives the phase velocity of the wave, while the imaginary part of αc represents the growth rate (positive if $\mathrm{Im}(\alpha c) > 0$).

Substitution of the streamfunctions $\Phi_j(x, y, t)$ into the linearized Navier–Stokes equations results in the well-known Orr–Sommerfeld equations for the y-dependent functions $\phi_j(y)$. Writing these equations in dimensionless form by scaling the length with the thickness of the film d_1, the velocity with the characteristic velocity $U_\tau = \tau d_1/\mu_1$ (recall that τ is defined as the shear force that the gas exerts on the liquid interface), the time with d_1/U_τ and the pressure with $\rho_1 U_\tau^2$ gives [4]

$$\phi_1'''' - 2\alpha^2\phi_1'' + \alpha^4\phi_1 = i\alpha R[(U_1 - c)(\phi_1'' - \alpha^2\phi_1) - U_1''\phi_1], \tag{2}$$

for the liquid film ($-1 < y < 0$), and

$$\phi_2'''' - 2\alpha^2\phi_2'' + \alpha^4\phi_2 = (i\alpha Rr/m)\,[(U_2 - c)(\phi_2'' - \alpha^2\phi_2) - U_2''\phi_2], \tag{3}$$

for the gas ($0 < y < \infty$). Primes are used to indicate differentation with respect to y, the liquid Reynolds number is defined as $R = \rho_1 U_\tau d_1/\mu_1$, and the density ratio r and the viscosity ratio m are defined as $r = \rho_2/\rho_1$ and $m = \mu_2/\mu_1$, respectively.

The boundary conditions expressing no-penetration and no-slip at the lower wall are

$$\phi_1 = \phi_1' = 0 \quad \text{at } y = -1. \tag{4}$$

Furthermore, the disturbances should be small far from the interface, which requires

$$\phi_2 = \phi_2' = 0 \quad \text{for } y \to \infty. \tag{5}$$

The conditions at the interface are the continuity of the velocity components and the balance of the stress components, both in the normal and tangential direction. This gives four conditions, which read [3, 4]

$$\phi_1 = \phi_2 \quad \text{at } y = 0, \tag{6}$$

$$\phi_1' + U_1'\phi_1/c = \phi_2' + U_2'\phi_2/c \quad \text{at } y = 0, \tag{7}$$

$$\phi_1'' + \alpha^2\phi_1 + U_1''\phi_1/c = m\,(\phi_2'' + \alpha^2\phi_2 + U_2''\phi_2/c) \quad \text{at } y = 0, \tag{8}$$

$$(\phi_1''' - 3\alpha^2\phi_1') + i\alpha R(c\phi_1' + U_1'\phi_1) - m(\phi_2''' - 3\alpha^2\phi_2') - ir\alpha R(c\phi_2' + U_2'\phi_2) - i\alpha R(F + \alpha^2 S)\,\phi_2/c = 0 \quad \text{at } y = 0, \tag{9}$$

where the inverse Weber number $S = \sigma/(\rho_1 U_\tau^2 d_1)$ and the inverse Froude number $F = g(\rho_1 - \rho_2)d/(\rho_1 U_\tau^2)$ are based on the interfacial tension σ and the gravitational acceleration g.

The primary flow $U_j(y)$ is specified as follows. Assuming smooth flow, the time-averaged velocity profile $U_2(y)$ of the turbulent gas can be approximated by [5]:

$$U_2(y) = y/m, \qquad 0 \le y \le s\mu_2/(d_1\sqrt{\rho_2\tau}),$$

$$U_2(y) = \sqrt{\tau/\rho_2}\,[s + (\gamma\tanh\tfrac{1}{2}\gamma)/\kappa]/U_\tau, \qquad y \ge s\mu_2/(d_1\sqrt{\rho_2\tau}),$$

$$\sinh\gamma = \frac{2\kappa d_1\sqrt{\rho_2\tau}}{\mu_2}\,[y - s\mu_2/(d_1\sqrt{\rho_2\tau})], \tag{10}$$

where we have distinguished a viscous sublayer (characterized by a linear profile) and a logarithmic part (i.e., it can be shown that for large y-values, $U_2(y)$ is approximately logarithmic in shape). The coefficient κ is the Von Kármán constant (often taken to be 0.4) and s determines the thickness of the viscous sublayer (often taken to be between 5 and 8). On a horizontal plate, the velocity in the liquid is linear (assuming laminar flow):

$$U_1(y) = y, \quad -1 \le y \le 0. \tag{11}$$

Note that we consider the problem in a frame that moves at the interfacial speed, i.e., $U_1 = U_2 := 0$ at $y = 0$.

Summarizing, it can be seen that the governing differential equations (2)–(3) can be used, together with the boundary and interface conditions (4)–(9), to provide a solution to the stability problem. The system (2)–(9) represents an eigenvalue problem so that the wave velocity c must take on specific values in order that the solution is nontrivial. Starting from the primary flow (10)–(11), we will discuss

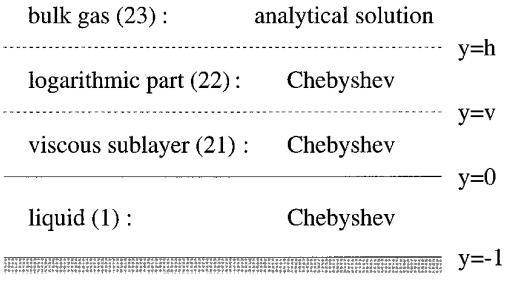

FIG. 2. For numerical convenience, the gas layer is divided into three parts: a part $y \geq h$ where the gas velocity is assumed to be constant; a logarithmic part $v \leq y \leq h$; and the viscous sublayer $0 \leq y \leq v$. The corresponding streamfunctions are denoted by $\psi_{23}(y)$, $\psi_{22}(y)$, and $\psi_{21}(y)$, respectively. The streamfunction $\psi_{23}(y)$ can be found analytically, while the streamfunctions $\psi_{22}(y)$ and $\psi_{21}(y)$, as well as the streamfunction in the liquid $\psi_1(y)$ are approximated by means of truncated Chebyshev series. The layers $y = h$ and $y = v$ are called "virtual" interfaces. We note that the figure is not on scale.

in the next section a collocation technique that provides the dispersion relation

$$c = c(\alpha, R, m, r, S, F), \tag{12}$$

together with the corresponding eigenfunctions $\phi_j(y)$. From the physical point of view, we are especially interested in eigenvalues with a positive imaginary part, since the stability of the flow is determined by the sign of the maximum of the growth rate, i.e., the sign of $\mathrm{Max}[\mathrm{Im}(\alpha c)]$.

3. NUMERICAL PROCEDURE

Several methods can be considered for solving the eigenvalue problem (2)–(9). For instance, we can try to solve the problem by means of a simple shooting method. However, practical difficulties then arise: the shooting technique requires a good initial guess of the eigenvalue and only a single eigenvalue is tracked. Another possibility is to make use of the compound matrix method as discussed by Ng and Reid [6, 7] and Yiantsios and Higgins [8]. Although this method is in general superior to shooting techniques [7], this method too does not provide the overall picture of the eigenvalue spectrum. Building upon the paper by Su and Khomami [9], as well as on our own experience [10], we therefore solve the eigenvalue problem by means of a Chebyshev collocation technique, which takes away the aforementioned difficulties. Moreover, unlike finite-difference approximations this method has the convenient property that it converges exponentially. We will now discuss this method in detail, using the conventions from Fig. 2.

Step 1. *Virtual interfaces.* To avoid numerical problems in the limit of large y-values, it is first assumed that the air velocity (10) remains constant above a certain height $y = h$, i.e., $U_2(y) = U_2(h) := U_{\max}$ for $y > h$. This allows for an analytical solution of the Orr–Sommerfeld equation (2) in the region $y > h$:

$$\phi_{23}(y) = De\alpha^{(h-y)} + Ee^{-\gamma(y-h)}, \tag{13}$$

where D and E are constants. The parameter γ is given by

$$\gamma^2 = (i\alpha Rr/m)(U_{\max} - c) + \alpha^2, \quad \mathrm{Re}(\gamma) > 0, \tag{14}$$

where Re( ) stands for taking the real part. The constraint $\mathrm{Re}(\gamma) > 0$ follows from the boundary conditions (5).

In order to reduce computing time, we also introduce a second "virtual" interface at the point $y = s\mu_2/(d_1\sqrt{\rho_2\tau}) := v$, where the air velocity (10) changes form a linear to a logarithmic shape. Due to this interface, the gas eigenfunctions $\phi_{21}(y)$ and $\phi_{22}(y)$ at either side of the interface can be approximated by a *different* number of Chebyshev polynomials (see Eq. (22) below). This is important because the logarithmic part is in general much thicker than the viscous sublayer and, as it turns out, the viscous sublayer always requires a certain minimum of polynomials before convergence is achieved. In fact, the introduction of the virtual interfaces in Fig. 2 is nothing but an application of the domain decomposition method (see, for instance, the book of Canuto, Hussaini, Quarteroni, and Zang [12], as well as the references therein) to the overall gas domain $[0, \infty)$; the gas domain is decomposed into the three subdomains $[0, v]$, $[v, h]$, and $[h, \infty)$.

At the two virtual interfaces $y = v$ and $y = h$, similar conditions as at the real interface hold. These conditions express continuity of velocity and stress and read in a general form [3, 11]:

$$\phi_{2k} = \phi_{2l}, \tag{15}$$

$$\phi'_{2k} + U'_{2k}\phi_{2k}/(c - U_{2k}) = \phi'_{2l} + U'_{2l}\phi_{2l}/(c - U_{2l}), \tag{16}$$

$$\phi''_{2k} + \alpha^2\phi_{2k} + U''_{2k}\phi_{2k}/(c - U_{2k}) = \phi''_{2l} + \alpha^2\phi_{2l} + U''_{2l}\phi_{2l}/(c - U_{2l}), \tag{17}$$

$$\phi'''_{2k} - 3\alpha^2\phi'_{2k} - 2\alpha^2U'_{2k}\phi_{2k}/(c - U_{2k}) = \phi'''_{2l} - 3\alpha^2\phi'_{2l} - 2\alpha^2U'_{2l}\phi_{2l}/(c - U_{2l}), \tag{18}$$

evaluated at $y = v$ with $k = 1$, $l = 2$, and at $y = h$ with $k = 2$, $l = 3$, respectively.

Step 2. *Chebyshev expansions.* Chebyshev polynomials are orthogonal on the interval $[-1, 1]$. Therefore, if we want to expand the eigenfunctions $\phi_1(y)$, $\phi_{21}(y)$, and $\phi_{22}(y)$ in terms of Chebyshev polynomials, we have to transform the Orr–Sommerfeld equations (2)–(3) on ei-

ther of the intervals $[-1, 0]$, $[0, v]$, and $[v, h]$ to the interval $[-1, 1]$ by a change of the independent variable y. This is easily achieved by means of the linear transformations

$$z = 2y + 1, \qquad -1 \le y \le 0, \tag{19}$$

$$z = -\frac{2y}{v} + 1, \qquad 0 \le y \le v, \tag{20}$$

$$z = \frac{2y - (h + v)}{(h - v)}, \qquad v \le y \le h. \tag{21}$$

After transforming the Orr–Sommerfeld equations in this way, we approximate the eigenfunctions $\phi_1(z)$, $\phi_{21}(z)$, and $\phi_{22}(z)$ by the truncated Chebyshev expansions

$$\begin{aligned} \phi_1^{(i)}(z) &= \sum_{n=0}^{N_1} a_n T_n^{(i)}(z), \quad \phi_{21}^{(i)}(z) = \sum_{n=0}^{N_{21}} b_n T_{\mathrm{n}}^{(i)}(z), \\ \phi_{22}^{(i)}(z) &= \sum_{n=0}^{N_{22}} c_n T_n^{(i)}(z), \end{aligned} \tag{22}$$

where $T_n(z)$ is the nth Chebyshev polynomial of the first kind, i denotes the ith derivative with respect to z, and a_n, b_n, and c_n are constants. The derivatives of the eigenfunctions can be found by differentiating the Chebyshev polynomials in (22). This is different from Orszag [13], who uses the properties of the Chebyshev polynomials (orthogonality conditions and recurrence relations) to arrive at expressions that do not contain derivatives of the Chebyshev polynomials. From our experience [3, 10, 14], however, we have learned that differentiation of the Chebyshev polynomials is much less involved and works well. It thus appears that even though this way of dealing with the derivatives of the streamfunctions reduces[1] the conditioning of the matrices involved in the resulting generalized eigenvalue problem (Eq. (26) below), the conditioning of these matrices is obviously not too bad in practice; when the generalized eigenvalue problem is treated in a careful manner (see steps 5 and 6), the eigenvalues and eigenvectors can be found within satisfactory accuracy for a large range of parameters. As we have shown explicitly in previous work [3, 10, 14], this accuracy can be checked by reproducing the asymptotic results of Yih [4, 11], Hooper and Boyd [15], and Van Gastel, Janssen, and Komen [23], among others.

Step 3. *Point collocation.* Once the Orr–Sommerfeld equations (2)–(3) have been transformed to the z-interval $[-1, 1]$, we collocate the approximations (22) at the extrema of the Chebyshev polynomials

$$z = \cos\left[\frac{\pi k}{M}\right], \quad k = 1, ..., M - 1, \tag{23}$$

as is characteristic for a Gauss–Lobatto grid [12], using the convention $M = N - 2$ with N equal to the number of polynomials N_1, N_{21}, N_{22}. This gives $N_1 - 3$, $N_{21} - 3$, and $N_{22} - 3$ equations for the expansion coefficients a_n, b_n, and c_n, respectively. The boundary conditions at $y = -1$ and the interface conditions at $y = 0$, $y = v$, and $y = h$ give the remaining equations that are required. More specifically, substitution of the expansions (22) and the exact solution (13) into the conditions (4), (6)–(9), and (15)–(18) gives 14 equations in terms of the coefficients a_n, b_n, and c_n and the constants D and E, which appear in the analytical solution (13). In total this gives $N_1 + N_{21} + N_{22} + 5$ equations for the $N_1 + N_{21} + N_{22} + 5$ unknowns a_n, b_n, c_n, D, E.

Step 4. *Generalized eigenvalue problem.* This system of equations, which is homogeneous and linear in a_n, b_n, c_n, D, E, also contains the eigenvalue c. To get the equations in a form that is linear in c, we first eliminate the term proportional to $1/c$ from the condition (9) at the real interface by means of (6) and (7), which gives a linear expression in c:

$$\begin{aligned} &(\phi_1''' - 3\alpha^2\phi_1') + i\alpha R(c\phi_1' + U_1'\phi_1) - m(\phi_2''' - 3\alpha^2\phi_2') \\ &\quad - ir\alpha R(c\phi_2' + U_2'\phi_2) + i\alpha R(F + \alpha^2 S) \\ &(\phi_1' - \phi_2')/(U_1' - U_2') = 0 \quad \text{at } y = 0. \end{aligned} \tag{24}$$

We note that it is thus not necessary to solve a nonlinear problem in c iteratively, as done by Valenzuela [16]. The only terms that are really nonlinear in c originate from the derivatives of ϕ_{23} in the virtual interface conditions (16)–(18) at $y = h$ (see Eqs. (13) and (14)). However, since the speed of the waves is usually much smaller than that of the maximum gas velocity, i.e., $|c| \ll U_{\max}$, we can replace (14) by

$$\gamma^2 = (i\alpha Rr/m)\, U_{\max} + \alpha^2, \quad \mathrm{Re}(\gamma) > 0, \tag{25}$$

which allows us to write the system of equations as a generalized eigenvalue problem:

$$[A]\mathbf{x} = c[B]\mathbf{x}, \tag{26}$$

where $\mathbf{x} = [a_0, ..., a_{N_1}, b_0, ..., b_{N_{21}}, c_0, ..., c_{N_{22}}, D, E]$. The correctness of the assumption $|c| \ll U_{\max}$ can be checked by solving the problem iteratively: (i) solve (26) with γ defined by (25); (ii) substitute the calculated eigenvalue in (14); and (iii) solve (26) again. In most cases, this shows that iteration does not significantly change the eigenvalues

[1] As is caused by the large matrix elements associated with the derivatives of the Chebyshev polynomials.

of interest. Obviously, in cases that the assumption does not prove to be correct, steps (ii) and (iii) should be repeated until convergence is achieved.

Step 5. *Elimination, balancing, and the QZ-algorithm.* The matrix B is singular, because some of the boundary and (virtual) interface conditions do not contain the eigenvalue c. Starting from the primary flow (10)–(11), it appears that there are in total 11 rows in B which are zero, corresponding to the following boundary and interface conditions: the two conditions (4) at the lower wall $y = -1$, the two conditions (6) and (8) at the real interface $y = 0$, the four conditions (15)–(18) at the virtual interface $y = v$, and finally[2] the three conditions (15), (17), and (18) at the virtual interface $y = h$. Due to these rows, the QZ-algorithm [17, 18] will give 11 infinite eigenvalues, which might interfere with the finite eigenvalues [19, 20]. We therefore eliminate the corresponding equations from the system, so that a smaller system of equations without the infinite eigenvalues is obtained:

$$[A']\mathbf{x}' = c[B']\mathbf{x}'. \tag{27}$$

Subsequently, because the new matrix A' can be ill-conditioned, we balance A' with the standard algorithm given by Osborne [21, 18]. This reduces the (Euclidean) norm of A', which is useful since the error produced by the QZ-algorithm is roughly proportional to this norm. We scale B' with the similarity transformation used for the balancing of A'. The resulting generalized eigenvalue problem

$$[A'']\mathbf{x}'' = c[B'']\mathbf{x}'' \tag{28}$$

is solved with the standard QZ-algorithm, which gives $\text{rank}(B'') = \text{rank}(B)$ finite eigenvalues. The eigenvalues c thus found are solutions of the original eigenvalue problem (26).

Step 6. *Original eigenvectors.* Due to the elimination of the infinite eigenvalues and the balancing of the matrix A', however, the computed eigenvectors $\mathbf{x}''$ are different from the eigenvectors $\mathbf{x}$ of the original problem (26). To reconstruct these original eigenvectors, the vectors $\mathbf{x}''$ must first be (back)transformed to the eigenvectors $\mathbf{x}'$ of the problem (27). This is achieved by means of the inverse of the similarity transformation used for the balancing of A'. The eleven rows in B which are zero then give the remaining equations that are required to compute the original eigenvectors $\mathbf{x}$. The eigenvectors $\mathbf{x}$ determine the streamfunctions $\Phi_j(x, y, t)$, as defined in Eq. (1), which contain all the information about the velocity and pressure disturbances in the linear stability problem.

[2] It should be noted that at the virtual interface $y = v$ both the first and the second derivatives of the velocity profile (10) are continuous and that at the virtual interface $y = h$ the term proportional to $1/c$ in the conditions (17) and (18) can be eliminated with the help of (16).

4. ILLUSTRATION OF NUMERICAL RESULTS

For a typical air–water system, the growth rate $\text{Im}(\alpha c)$ as a function of the wavenumber α is shown in Fig. 3. The liquid Reynolds number $R = 400$ and the shear stress $\tau = 19.2\ N/m^2$ correspond to a friction velocity $u^* = (\tau/\rho_2)^{1/2} = 4\ m/s$, an interfacial speed $U_i = 2.77$ m/s and a film thickness $d_2 = 0.144$ mm [3]. For the parameters used, convergence is achieved for $N_1 = 20$, $N_{21} = 10$, and $N_{22} = 50$; i.e., using more polynomials does not affect the first three digits of the most unstable eigenvalue (Table I). The parameter $y = h$, above which the air velocity (10) is assumed to be constant, has been varied in such a way that the growth rate becomes independent of it (this yields $h \geq 2$, according to Table II). We found that if the streamfunction on the y-interval $[0, h]$ had been described by a *single* Chebyshev expansion, at least 360 polynomials would have been required before the first three digits in c can be considered significant. These digits are the same as those in Table I, which shows that the error caused by introducing the virtual interface $y = v$ is negligible, as should be the case (recall that this interface does not have any physical meaning at all). Because the computing time taken by the QZ-algorithm is proportional to N^3, with N the order of the matrices A'' and B'', the above example illustrates the convenience of introducing a second virtual interface $y = v$.

Figure 3 shows that for a single set of parameters, *two* modes of instability can be unstable. Although the growth rate of the second mode (dashed line) is an order of magnitude smaller than that of the first mode (solid line), it can be argued [3] that its dimensional growth rate is, in principle, still large enough to be observed. Consequently, the second mode should not be neglected in interpreting experiments *a priori*. From a computational point of view, this feature stresses the importance of having at one's disposal a robust numerical code that does not only track a single eigenvalue, but returns approximations to more than just one eigenvalue. This reduces the risk of missing unstable modes of instability.

The two modes of instability in Fig. 3 differ in their position of the critical layer, i.e., the plane where the wave velocity $\text{Re}(c)$ is equal to the velocity of the primary flow. While the critical layer for the first mode is directly above the interface ("interfacial mode," $\text{Re}(c) > 0$), it is for the second mode in the bulk of the liquid film ("internal mode," $\text{Re}(c) < 0$. The streamfunctions corresponding to the interfacial and the internal mode are given in Figs. 4 and 5, respectively. It is seen that, whereas the streamfunction for the interfacial mode is characterized by a small,

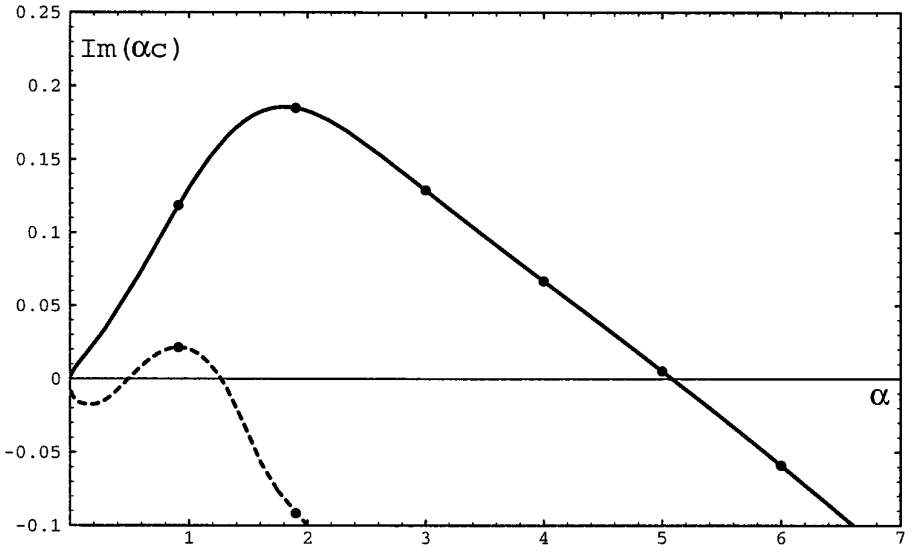

FIG. 3. The growth rate Im(αc) of the first mode (solid line) and the second mode (dashed line) as a function of the wavenumber α for a typical air-water system ($R = 400$, $m = 0.018$, $r = 0.0012$, $S = 6.68\ 10^{-2}$, $F = 1.84\ 10^{-4}$). These curves have been calculated numerically from the dispersion relation (12), using 20 polynomials in the liquid film $-1 \le y \le 0$, 10 in the viscous sublayer $0 \le y \le v$, and 50 in the logarithmic part $v \le y \le h$ (cf. Table I). We note that without the use of a virtual interface $y = v$, at least 360 polynomials would have been required in the region $0 \le y \le y$. The dots represent results obtained when calculations are done in the latter way.

but positive real part in the liquid film, this part is negative for the internal mode.

By means of the streamfunction it is for instance possible to make contour plots of the velocity, pressure, and stress disturbances in the two fluids, thus providing physical insight into the wave-induced flow field. This is illustrated in Fig. 6 for the pressure distribution $p_j(x, y)$ corresponding to the interfacial mode, keeping the time t fixed. The figure is based on the fact that the pressure field $p_j(x, y, t)$ can be related directly to the streamfunction $\Phi_j(x, y, t)$ [4],

$$p_1(x, y, t) = -(U_1 - c)\Phi_1' + U_1'\Phi_1 + (1/(i\alpha R))\,(\Phi_1''' - \alpha^2\Phi_1'), \tag{29}$$

in the liquid film ($-1 < y < 0$), and

$$p_2(x, y, t) = r[-(U_2 - c)\Phi_2' + U_2'\Phi_2 + (m/(i\alpha Rr))\,(\Phi_2''' - \alpha^2\Phi_2')], \tag{30}$$

in the gas ($0 < y < \infty$). Notice that only the real part of these expressions can be ascribed physical meaning.

TABLE I

Convergence of the Real and the Imaginary Parts of the Eigenvalue c for $\alpha = 1.90$, $R = 400$, $m = 0.018$, $r = 0.0012$, $S = 6.68\ 10^{-2}$, $F = 1.84\ 10^{-4}$, $h = 2$

N_1	N_{21}	N_{22}	Re(c)	Im(c)
10	10	20	0.0968	0.0959
15	15	30	0.0949	0.0976
20	20	40	0.0949	0.0973
25	25	50	0.0949	0.0973
25	10	50	0.0949	0.0973
10	10	50	0.0963	0.0964
20	10	50	0.0949	0.0973
20	15	50	0.0949	0.0973
20	10	75	0.0949	0.0973

Note. The wavenumber corresponds to the maximum of the growth rate of the interfacial mode in Fig. 3. Computation of three significant digits in c requires 20 polynomials in the liquid film, 10 in the viscous sublayer, and 50 in the logarithmic part of the gas velocity profile.

TABLE II

Convergence of the Real and the Imaginary Parts of the Eigenvalue c, Varying the Distance h from the Interface above which the Air Velocity Is Assumed to Be Constant

h	Re(c)	Im(c)
0.25	0.0950	0.0782
0.5	0.0948	0.0942
1.0	0.0948	0.0971
2.0	0.0949	0.0973
4.0	0.0949	0.0973

Note. The parameters used are $\alpha = 1.90$, $R = 400$, $m = 0.018$, $r = 0.0012$, $S = 6.68\ 10^{-2}$, $F = 1.84\ 10^{-4}$, $N_1 = 20$, $N_{21} = 10$, $N_{22} = 50$ (cf. Table I), except for the case $h = 4$, where we have used $N_{22} = 70$. Three sigificant digits in c are achieved for $h \ge 2$.

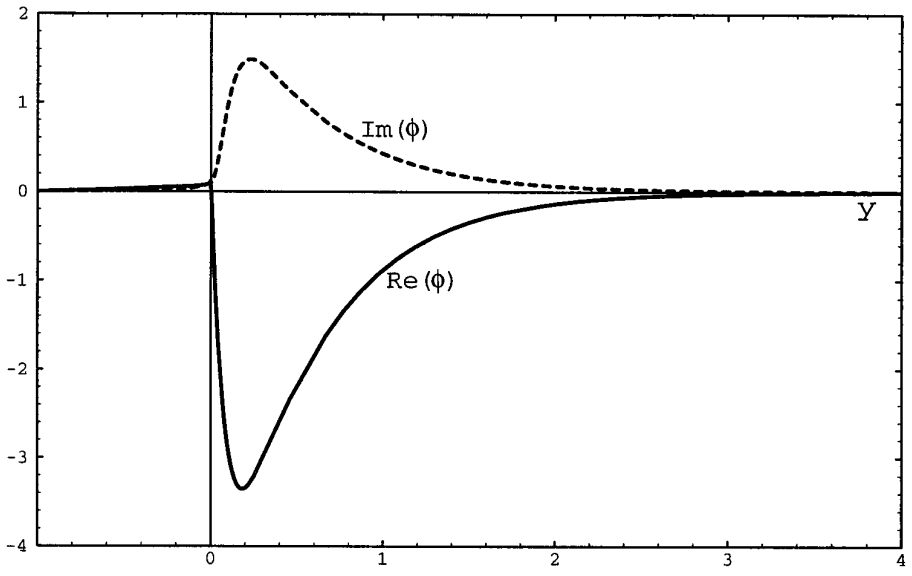

FIG. 4. The real and the imaginary parts of the streamfunction for the first mode of instability ('interfacial mode') in Fig. 3, evaluated for the most unstable wavenumber $\alpha = 1.90$. Because of the arbitrary normalization of the streamfunction in linear theory, the vertical scale is arbitrary. We note that when the streamfunction is known, it is possible to obtain insight in the physical mechanism by which energy is being transferred from the primary to the disturbed low (for details see [14]).

In a first approximation, as indicated by the inviscid Bernoulli equation [22], we may expect the pressure disturbances in the gas to be more or less out-of-phase with the wave height because the gas streamlines are compressed in the crest region and expanded in the trough region. Although this effect of suction can readily be recognized in Fig. 6, it is clear that the pressure distribution has a substantial component in phase with the wave slope as well. As shown asymptotically by Benjamin [2] for a gas flow over a solid wavy boundary, this ''quasi-sheltering'' effect is caused by the presence of a viscous friction layer located directly above the interface. It is called ''quasi-

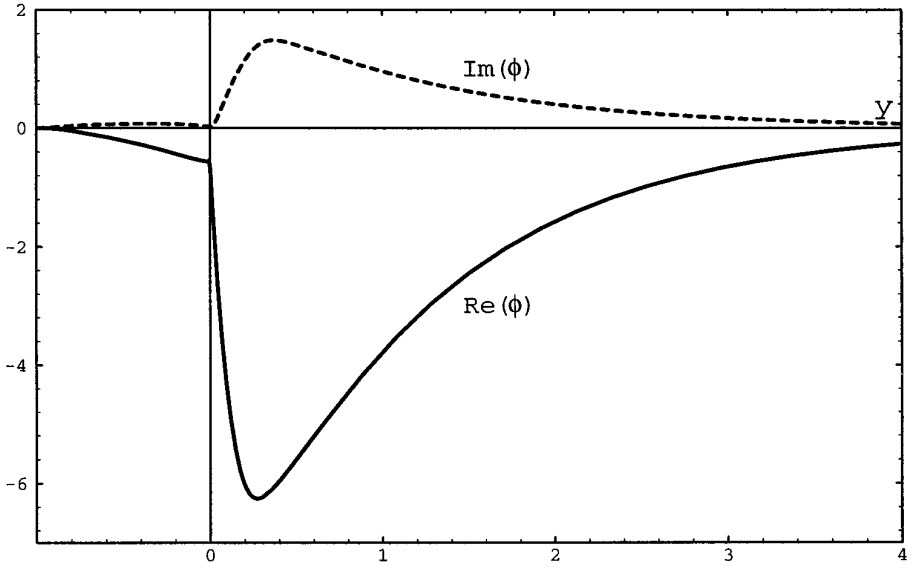

FIG. 5. The real and the imaginary part of the streamfunction for the second mode of instability ('internal mode') in Fig. 3, evaluated for the most unstable wavenumber $\alpha = 0.91$.

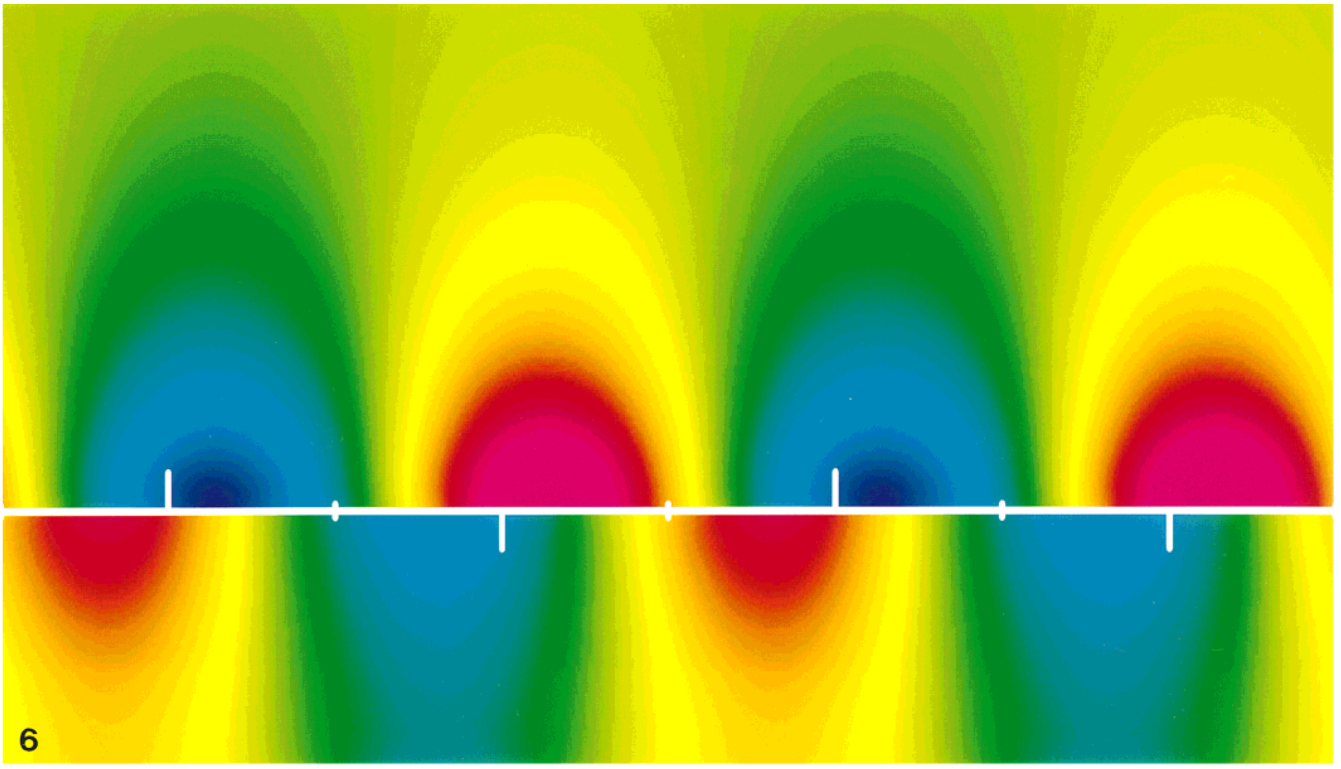

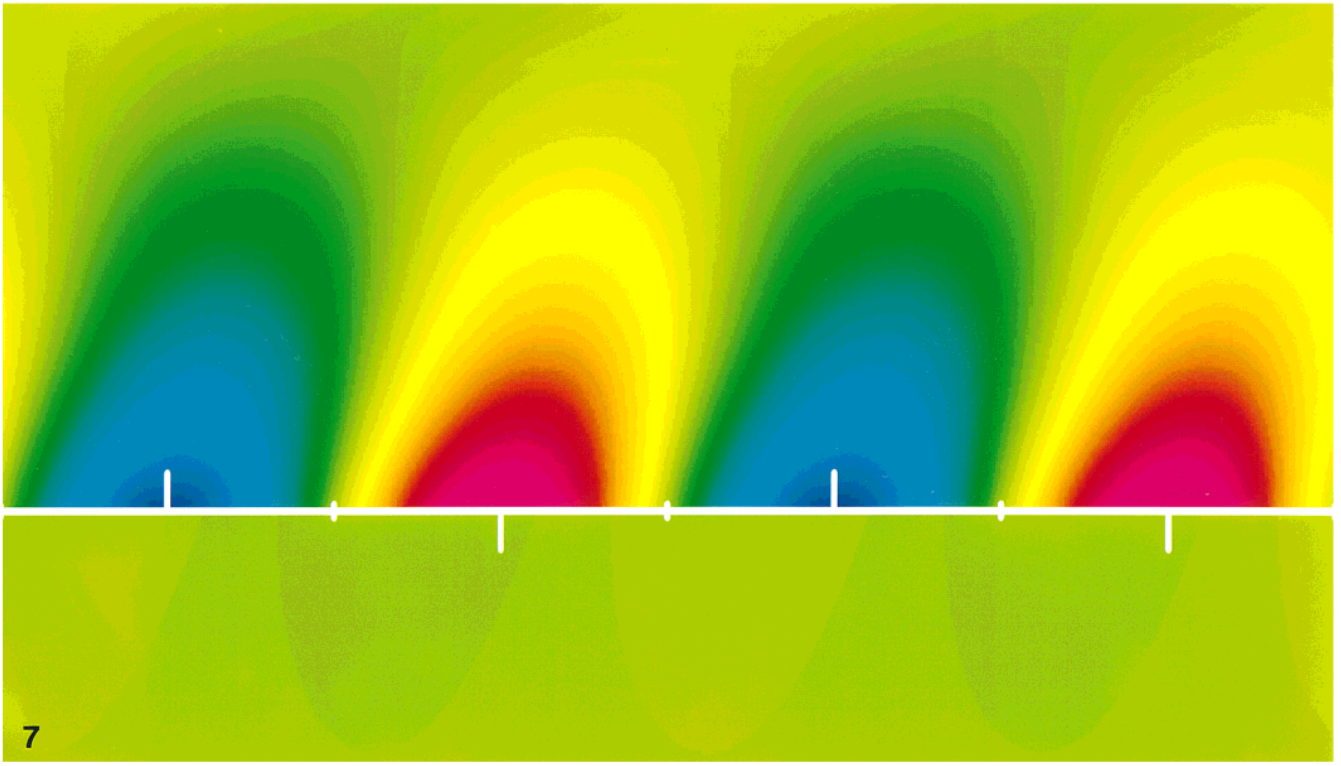

FIG. 6. Distribution of the pressure disturbances $p_j(x, y)$ for the interfacial mode shown in Fig. 3, evaluated for the most unstable wavenumber $\alpha = 1.90$. The width corresponds to exactly two wavelengths: the white tick marks indicate the position of the zeros and the extrema of the simple-harmonic wavy interface disturbance $y = \hat{\eta} \sin(\alpha x)$. The white line represents the undisturbed interface $y = 0$; the vertical coordinate ranges from the boundary wall $y = -1$ to an arbitrary chosen truncation height $y = 2$. The pressure disturbances, as calculated from the streamfunction $\Phi_j(x, y, t)$ for a fixed value of the time t, are largely negative in the blue regions and largely positive in the red regions. Relative to the wavy interface, the primary flow is in the gas directed from the left to the right and in the liquid just the other way around. Note that in both fluids the pressure attains its minimum at the downstream side of the interface displacement.

sheltering'' because the features in Fig. 6 have the same general character as if the flow were separated on the downstream side, i.e., just as if a wake were formed behind each wave crest (The term sheltering usually refers to the flow about a solid body in an otherwise uniform stream of fluid. Under certain conditions a wake is then formed behind the body, thus causing a (permanent) loss in pressure [22]). A similar effect can be observed at the liquid side of the wavy interface, realizing that relative to the interface the liquid flows from the right to the left (i.e., the liquid moves slower to the right than the waves do; Re(c) is positive).

Figure 7 gives an impression of the field $u_j(x, y)$ of the velocity disturbances in the tangential direction, i.e., in the direction of the primary flow. The figure can be derived directly from the streamfunction $\Phi_j(x, y, t)$ according to the definition $u_j = \partial\Phi_j/\partial y$, keeping the time t fixed. Obviously, the velocity disturbances in the gas are much larger than those in the liquid and are almost out-of-phase with the wave height. This can readily be understood from the interface condition expressing continuity of tangential velocity, Eq. (7), using the fact that the viscosity difference between the two fluids causes the slope of the basic-state velocity profile at the interface to be much larger in the air than in the liquid (Fig. 1). Consequently, when the interface is being deformed, it will primarily be the velocity disturbances in the gas, and not those in the liquid, that must compensate for the gap in the velocity of the primary flow. In terms of the interface condition (7), this implies $u_2 \approx -\eta U_2'$ at $y = 0$.

In addition, we note that the difference in the vertical scales in Figs. 6 and 7 suggests that the pressure disturbances at the interface are the result of a cumulative action over the whole flow field, while at the same time the velocity disturbances seem to depend mainly on the local state of affairs (although not shown here, this also holds for the disturbances in the shear stress). This feature in fact provides another visualization of the just-mentioned work of Benjamin [2]. In his paper, Benjamin gives asymptotic expressions for the pressure distribution at the interface in terms of the *integral* of the streamfunction over the whole gas layer, while in contrast the expressions for the velocity and the shear stress distributions depend on the local value of the streamfunction only.

For a more searching discussion of the physical aspects of the linear stability problem, which is beyond the scope of the present paper, we refer to [14].

5. CONCLUDING REMARKS

In the foregoing we have considered the specific problem of a thin film of liquid sheared by a gas. The numerical techniques discussed, however, can readily be applied to other two-phase flow configurations as well. For instance, by choosing the thickness of the fluid layer d_1 a few times larger than the length of the disturbance, the situation corresponds to the problem of the generation of waves on deep water. In this situation, the wind-induced current $U_1(y)$ can be approximated by

$$U_1(y) = (U_0/U_i)[e^{(U_i y/U_0)} - 1], \tag{31}$$

where U_0 is the interfacial speed, having a value of typically 60% of the friction velocity $u_* = \sqrt{\tau/\rho_1}$ [23]. After replacing the linear profile (11) in the existing computer code by this new one, the film thickness d_1 is then varied in such a way that the (dimensional) growth rate becomes independent of it. This shows, among others, that the interfacial mode in Fig. 3 manifests itself in the context of deep water as so-called capillary-gravity waves, with a wavelength of typically 1 *cm* (for more details, see [3]).

Once one has some experience with the Chebyshev collocation method in the context of a sheared liquid film, solving the stability problem of parallel two-phase flow in a much more *general* sense is in fact straightforward. Here, two-phase flow means both liquid–liquid as well as gas–liquid flow and includes widely divergent flow systems like, for instance, wind over the surface of the ocean, plane Couette–Poiseuille flow in a channel and film flow down an inclined plane. A good starting point for solving the generalized stability problem is to consider parallel two-phase flow in an inclined channel. In addition to the conventions introduced before, this involves the introduction of two new symbols: β, the angle of inclination of the flow configuration, and $n = d_2/d_1$, which denotes the ratio of the layer thickness of the upper fluid $j = 2$ and the lower fluid $j = 1$. In line with the above, unbounded flow is described by taking a very large value for the layer thickness of the fluid in question. When the primary flow $U_j(y)$, which is driven by a pressure gradient, by a shear stress or by gravity, is known, the stability problem is described by two Orr–Sommerfeld equations, four boundary conditions, and four interface conditions. It will be clear that the dispersion relation

FIG. 7. Distribution of the tangential velocity disturbances $u_j(x, y)$ for the interfacial mode shown in Fig. 3, evaluated for the most unstable wavenumber $\alpha = 1.90$. The vertical scale extends from $y = -0.1$ to $y = 0.2$, while other conventions used are the same as those in Fig. 6. The disturbances are largely negative in the blue regions and largely positive in the red regions. Due to the low viscosity of the air, the disturbances are the largest in the gas and approximately out-of-phase with the wave height.

$$c = c(\alpha, R, m, r, n, S, F, \beta), \tag{32}$$

can then be computed from a modified version of the computer code solving the thin film problem. Starting from the corresponding eigenfunctions, we have recently been able to present a classification scheme for the various instabilities arising in parallel two-phase flow [14].

We finally draw attention to the fact that we have examined the stability of fluid flow by testing for "unstable" eigenvalues of the linearized equations of motion. Recently, however, several researchers have questioned the use of eigenvalue analysis for examining hydrodynamic stability (see, for instance, Trefethen, Trefethen, Reddy, and Driscoll [24]). These researchers claim that when the eigenfunctions are not orthogonal to one another [25], it is still possible to have disturbance growth even if all eigenmodes are stable. Some evidence for this may be found in the well-known fact that the predictions of eigenvalue analysis fail to match experiment for flow configurations like single-phase Poiseuille and Couette flow in a channel [24]. At the same time, however, it should be realized that while the predictions of eigenvalue analysis are quite unsatisfactory for some flows, they obviously *do* match experiment for other flows (like the flow of a thin film of liquid sheared by a gas,[3] as discussed above [3]). As suggested by Hooper and South [27], among others, the possibility of nonnormal growth is likely to play a role only if the eigenvalue distribution over the complex plane is characterized by a certain degree of clustering. Running ahead on further research on this topic, we anticipate that the collocation Chebyshev technique described in this paper can also be used for analyzing nonmodal growth, for instance by visualizing the eigenvalue distribution over the complex plane.

[3] For other examples in the context of parallel two-phase flow, we refer to the book of Joseph and Renardy [26].

REFERENCES

1. P. G. Drazin and W. H. Reid, *Hydrodynamic Stability* (Cambridge Univ. Press, Cambridge, 1981).
2. T. B. Benjamin, *J. Fluid Mech.* **6,** 161 (1959).
3. R. H. M. Miesen and B. J. Boersma, *J. Fluid Mech.* **301,** 175 (1995).
4. C.-S. Yih, *J. Fluid Mech.* **27,** 337 (1967).
5. J. W. Miles, *J. Fluid Mech.* **13,** 433 (1962).
6. B. S. Ng and W. H. Reid, *J. Comput. Phys.* **33,** 70 (1979).
7. B. S. Ng and W. H. Reid, *J. Comput. Phys.* **58,** 209 (1985).
8. S. G. Yiantsios and B. G. Higgins, *J. Comput. Phys.* **74,** 25 (1988).
9. Y. Y. Su and B. Khomami, *J. Comput. Phys.* **100,** 297 (1992).
10. R. H. M. Miesen, G. Beijnon, P. E. M. Duijvestijn, R. V. A. Oliemans, and T. M. M. Verheggen, *J. Fluid Mech.* **238,** 97 (1992).
11. C.-S. Yih, *J. Fluid Mech.* **212,** 41 (1990).
12. C. Canuto, M. Y. Hussaini, A. Quarteroni, and T. A. Zang, *Spectral Methods for Fluid Dynamics* (Springer-Verlag, New York, 1988).
13. S. A. Orszag, *J. Fluid Mech.* **50,** 689 (1971).
14. P. A. M. Boomkamp and R. H. M. Miesen, *Int. J. Multiphase Flow,* submitted.
15. A. P. Hooper and W. G. C. Boyd, *J. Fluid Mech.* **128,** 507 (1983).
16. G. R. Valenzuela, *J. Fluid Mech.* **76,** 229 (1976).
17. C. B. Molar and G. W. Stewart, *SIAM J. Numer. Anal.* **10,** 241 (1973).
18. G. Golub and C. van Loan, *Matrix Computations* (Johns Hopkins Univ. Press, London, 1989).
19. J. Gary and R. Helgason, *J. Comput. Phys.* **5,** 169 (1970).
20. D. A. Goussis and A. J. Pearlstein, *J. Comput. Phys.* **84,** 242 (1989).
21. E. E. Osborne, *J. Assoc. Comput.* **7,** 338 (1960).
22. G. K. Batchelor, *An Introduction to Fluid Dynamics* (Cambridge Univ. Press, Cambridge, 1990).
23. K. van Gastel, P. A. E. M. Janssen, and G. J. Komen, *J. Fluid Mech.* **161,** 199 (1985).
24. L. N. Trefethen, A. E. Trefethen, S. C. Reddy, and T. A. Driscoll, *Science* **261,** 578 (1993).
25. S. C. Reddy, P. J. Schmid, and D. S. Henningson, *SIAM J. Appl. Math.* **53,** 15 (1993).
26. D. D. Joseph and Y. Y. Renardy, *Fundamentals of Two-Fluid Dynamics, Part II*: *Lubricated Transport, Drops and Miscible Fluids* (Springer-Verlag, New York, 1993).
27. A. P. Hooper and M. South, *Eigenvalues and Disturbance Growth in Channel Flows of Two Superposed Viscous Fluids* (Research and Consultancy Report 4, Faculty of Computer Studies and Mathematics, University of the West of England, Bristol 1995).